Studies of the Lowest Excited Triplet State of 3,3′-Biisoquinoline(dicyano)platinum(II) [Pt(CN)$_2$(*i*-biq)] by Means of Time-Resolved Electron Paramagnetic Resonance and Optical Spectroscopy

Tomoyo Funayama, Masako Kato,† Hiroshi Kosugi, Mikio Yagi,†† Jiro Higuchi,†† and Seigo Yamauchi*

Institute for Chemical Reaction Science, Tohoku University, Katahira 2-1-1, Aoba-ku, Sendai 980-8577

†Division of Material Science, Graduate School of Human Culture, Nara Women's University, Nara 630-8506 and PRESTO, JST, Kawaguchi 332-0012

††Department of Applied Chemistry, Faculty of Engineering, Yokohama National University, Tokiwadai, Hodogaya-ku, Yokohama 240-8501

(Received December 7, 1999)

The lowest excited triplet (T_1) state of 3,3′-biisoquinoline(dicyano)platinum(II), [Pt(CN)$_2$(*i*-biq)] was examined by time-resolved electron paramagnetic resonance (TREPR) and optical techniques in comparison with that of a ligand 3,3′-biisoquinoline (*i*-biq). *Trans* and *cis* *i*-biqs were assigned from obtained and calculated zero-field splittings (zfs') in the T_1 state. The zfs parameter D increased with complex formation from 2.66 to 4.66 GHz in a rigid dimethylformamide solution; the polarization pattern of the spectrum was very different between the ligand and the complex. The triplet lifetime (ca. 1 s) of *i*-biq is also remarkably shortened in the complex (ca. 2 ms). These facts were analyzed in terms of the spin-orbit coupling (soc) between T_1 ($\pi\pi^*$) and $^{1,3}d\pi^*$. From the analyses, the soc matrix element and the magnitude of delocalization of π^* electrons over the Pt atom are obtained as 65 cm^{-1} and 0.02, respectively. The solvent dependences of the D value and the triplet lifetime also support the importance of the $^{1,3}d\pi^*$ states for the T_1 ($\pi\pi^*$) properties of the complex.

The lowest excited states are very important, for their lifetimes are the longest among the excited states; they determine the properties of emissions and lifetimes of the excited states and suffer from various kinds of chemical reactions depending on their characters. In metal complexes, the nature of the lowest excited triplet (T_1) state varies with combination of a central metal, a ligand, and a counter ion, showing $\pi\pi^*$, $d\pi^*$, and dd characters. Extensive studies were reported on the T_1 states of metal complexes involving α-diimine ligands owing to their utilities as photosensitizers in energy transfer and/or electron transfer reactions.[1,2]

In these studies, quantitative characterization of the state was essential and has been examined by various parameters and techniques. Among those, properties of the triplet sublevels including zero-field splittings (zfs'), a g-value, and an $S_1 \rightarrow T_1$ intersystem crossing (isc) rate, which are obtained by an electron paramagnetic resonance (EPR) technique, often provide unique and valuable information on the T_1 state. Especially in a case where a mixing occurs between the excited states, these parameters are very useful in elucidating a mixed character. This method was applied for the first time to studies of the metal complex by Komada et al. in 1986[3] by means of an optically detected zero-field magnetic resonance (ODMR) technique. Thereafter, several ODMR and time-resolved EPR (TREPR) studies have been reported on metal complexes such as Rh, Ru, Cd, Zn, and Re complexes, whose T_1 states provide similar properties to those of the ligands and show almost pure $\pi\pi^*$ character.[3—9]

In this report, we extend the study to a mixed state of $^3\pi\pi^*$ and $^3d\pi^*$ in the T_1 state of the metal complex. Among the metal complexes reported so far, platinum (Pt) α-diimine complexes are considered to have mixed characters on the basis of their phosphorescence spectra and triplet lifetimes. We selected [Pt(CN)$_2$(*i*-biq)] as a model system having a mixed $^3\pi\pi^*$–$^3d\pi^*$ character. Kato et al. reported the optical properties for this system and have assigned the T_1 state as $^3\pi\pi^*$.[10]

We obtained EPR parameters and an isc ratio from the analyses of TREPR spectra and determined energy levels of the excited states from emission, excitation, and absorption spectra. On the basis of these data, the T_1 properties are interpreted in terms of a mixing between the $^3\pi\pi^*$ and $^{1,3}d\pi^*$ states via a spin-orbit coupling (soc). We also analyze the triplet properties of the ligand *i*-biq including assignment of *trans* and *cis* conformers.

The fine structure axes are taken as shown in Fig. 1, where

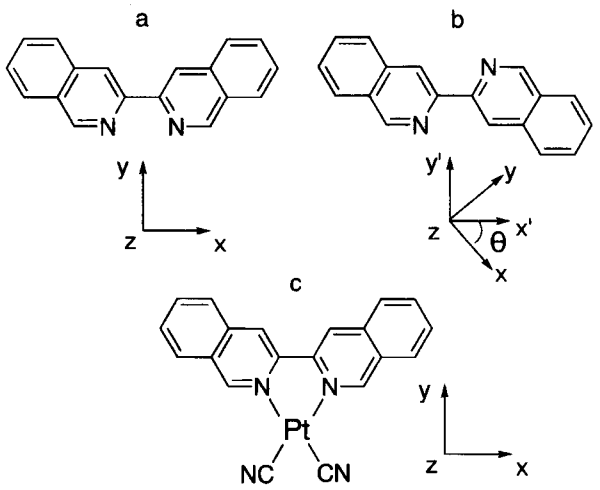

Fig. 1. Molecules and fine structure axes (x, y, z) for (a) *cis*-, (b) *trans*-3,3′-biisoquinoline (*i*-biq), and (c) [Pt(CN)$_2$ (*i*-biq)]. See the next for θ.

the z axis is perpendicular to the plane.

Experimental

Materials. The ligand molecule *i*-biq was synthesized from 3-bromoisoquinoline (briq),[11] which is obtained by consecutive syntheses of homophthalimide[12] and 1,3-dibromoisoquinoline.[13] We used the following method for 3,3′,4,4′-tetramethoxy-2,2′-bipyridyl.[14] $NiCl_2 \cdot 6H_2O$ (0.896 g, 3.77 mmol) and triphenylphosphine (3.955 g, 15.1 mmol) were stirred in dimethylformamide (DMF; 18.8 ml) under nitrogen atmosphere. Activated Zn[15] (0.246 g, 3.76 mmol) was added to this blue-colored solution, which was stirred for an hour at 50 °C under nitrogen atmosphere, giving a prompt color change from blue to wine red. Then briq (0.784 g, 3.77 mmol) in DMF (2.8 ml) was added to the solution, which was refluxed for one and half hours at the same temperature under nitrogen atmosphere and then poured into an aqueous (5.6%) ammonium solution (50 ml) in air. After extraction from chloroform four times, *i*-biq was obtained by column chromatography of silica gel using chloroform as eluent. The pale yellow product of ca. 80% yield was purified by recrystallization from methanol. The compound was further purified by HPLC through silica gel column using hexane and acetic acid (1 : 1) with 3% triethylamine as eluent. The colorless needle-shaped crystals were finally obtained.

[Pt(CN)$_2$(*i*-biq)][10] (*i*-biq complex) and [Pt(CN)$_2$(bpy)][16] (bpy complex) were prepared according to the methods described in the literature and were recrystallized from DMF.

Measurements. The solutions for low temperature measurements were deareated by repeated freeze-pump-thaw cycles using a vacuum line. The crystalline samples were made by pasting the crushed crystal on a quartz plate. UV-vis absorption spectra were observed on Shimadzu UV-160A spectrophotometer at room temperature. Phosphorescence emission and its excitation spectra were obtained at room temperature and at 77 K with a Hitachi 850 fluorescence spectrophotometer equipped with a Hamamatsu R928 photomultiplier. The excitation spectra were corrected with the Rhodamine B solution. A triplet lifetime was measured from the decay of phosphorescence by using an electric shutter or a laser pulse. Each decay curve was stored on an Iwatsu DM7200 digital memory. The concentrations of the samples were 1×10^{-5} mol dm^{-3} and 5×10^{-6} mol dm^{-3} for *i*-biq and the complexes, respectively. TREPR spectra were observed on a JEOL FE2X EPR spectrometer by an NF BX-531 boxcar integrator without field modulation. The samples were excited at 308 nm by a Lamda Physik LPX 100i excimer (XeCl) laser. Temperature was controlled by using an Oxford ITC4 cryo-system at 20—120 K. Magnetophotoselection (MPS) experiments were made by using a Glan–Thompson polarizer and the unpolarized excimer laser. For these EPR experiments, the concentrations of the samples were 5×10^{-4} mol dm^{-3} and 5×10^{-6}—5×10^{-4} mol dm^{-3} for *i*-biq and the complexes, respectively.

Results and Interpretation

We first examine the excited states of the ligand, *i*-biq, by means of optical and TREPR spectroscopy and compare the results with those of the Pt complex.

1. 3,3′-Biisoquinoline. As *trans* and *cis* conformers are expected to be involved in *i*-biq such as cases of 2,2′-bipyridine (bpy) and 2,2′-biquinoline (bq), solvent dependences were analyzed on their optical and EPR properties of the T_1 states.[17—25] Two kinds of solvents, ethanol and acidic ethanol including 2.02 wt% H_2SO_4, were used as typical solvents for two conformers, based on previous studies.[17—19]

1.1. Optical Properties. An absorption spectrum of *i*-biq was observed in ethanol and the peak in the longest wavelength region was shifted to the red by adding acid into ethanol, where the bands rise at 365 and 400 nm (Fig. 2), respectively. Isosbestic points were observed at 253, 280, and 332 nm in these solvents. These results are similar to those of bpy[17,18] and bq[18] reported previously and suggest involvements of *trans* and *cis* isomers, which are discussed in the following section. Phosphorescence spectra were observed at 77 K, as shown in Fig. 3, and also red-shifted (ca. 450 cm^{-1}) in acidic solvent. Vibrational analyses of the spectra are summarized in Table 1. The energies of the S_1 states were determined from an overlap of the absorption and fluorescence spectra (Fig. 2) as 28000 cm^{-1} (ε = 1000 mol^{-1} dm^3 cm^{-1}) and 25950 cm^{-1} (ε = 4200 mol^{-1} dm^3 cm^{-1}) in both solvents. The phosphorescence was weaker and the lifetime shorter (1.0 s vs. 1.3 s) in acidic ethanol. Based on these properties, the S_1 and T_1 states are assigned to be $\pi\pi^*$ in nature.

We examined *i*-biq in ethanol including 12.1 wt% ethyl iodide, because Belser et al.[26] reported that the *cis* form is stable in this system. It was found that the phosphorescence spectra (Fig. 3 and Table 1) and the lifetime (0.27 s) are different from those in neat ethanol, but the T_1 energy is nearly the same.

1.2. EPR Properties. TREPR spectra were observed at 73 K and 0.8 μs after the laser pulse in both solvents, as shown in Figs. 4 and 5. The polarization pattern is different depending on the solvent, showing E, AEA/EAE and E, EEE/AAA from the low to high fields in neat and acidic ethanol, respectively. E and A denote an emission and an absorption of microwave and are shown at the stationary fields in the figure. These spectra were easily simulated with the parameters summarized in Table 2, giving rise to two possible parameter sets having different orders of triplet sublevels in both systems; $D \equiv (-3/2)Z > 0$ with P_x, $P_y >$

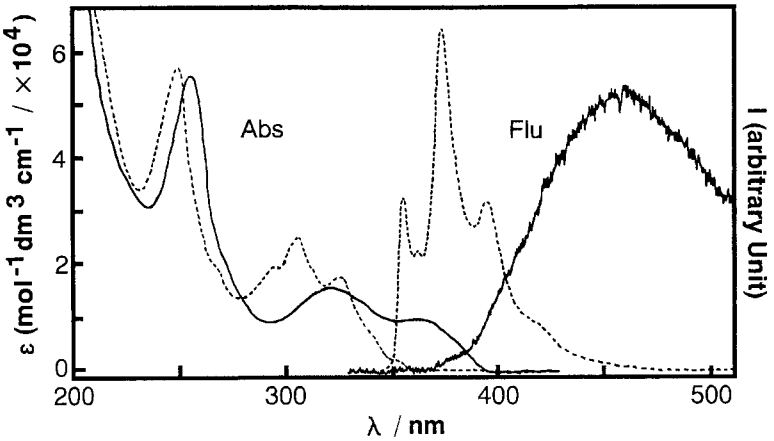

Fig. 2. Absorption (Abs) and fluorescence (Flu) spectra of 3,3′-biisoquinoline in neat ethanol (- - -) and in acidic ethanol with H_2SO_4 (2.02 wt%) (——) observed at room temperature.

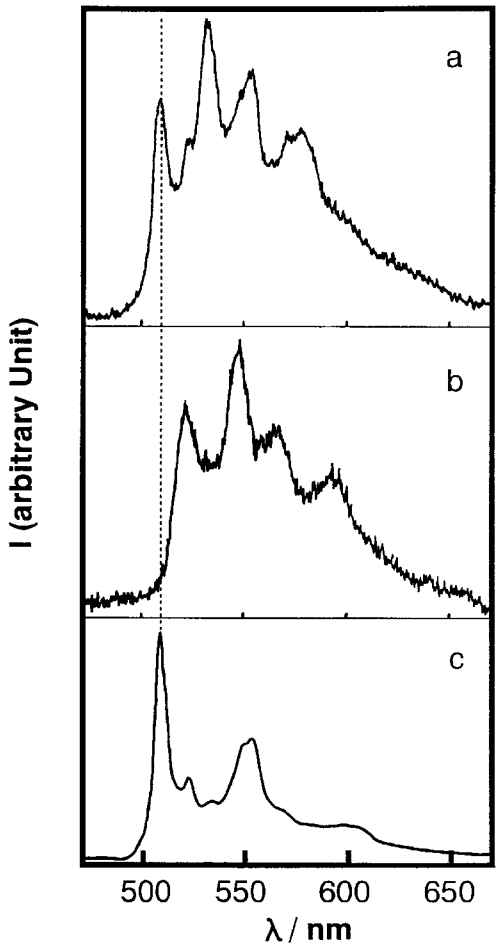

Fig. 3. Phosphorescence spectra of 3,3′-biisoquinoline in (a) neat ethanol and in (b) acidic ethanol, and in (c) ethanol with ethyl iodine (12.1 wt%) observed at 77 K.

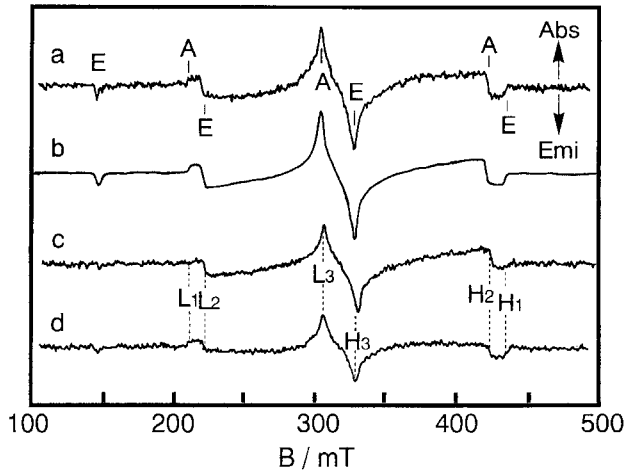

Fig. 4. Time-resolved EPR spectrum (a) of 3,3′-biisoquinoline observed in ethanol at 73 K and 0.8 μs after the laser pulse, the simulation spectrum (b) using parameters summarized in Table 2, and magnetophotoselection spectra under excitation with (c) $\boldsymbol{E}\perp\boldsymbol{B}$ and (d) $\boldsymbol{E}\|\boldsymbol{B}$ at 308 nm.

P_z and $D < 0$ with $P_z > P_x, P_y$ where Z is the energy of the T_z sublevel.

In order to assign the triplet sublevel, we made MPS experiments using unpolarized light (λ = 308 nm) of the laser and the polarizer. The MPS spectra were observed with $\boldsymbol{E}\|\boldsymbol{B}$ and $\boldsymbol{E}\perp\boldsymbol{B}$ as shown in Figs. 4 and 5, where $\boldsymbol{E}$ and $\boldsymbol{B}$ denote the direction of polarized light and that of the magnetic field, respectively. In ethanol, three sets of stationary peaks, L_1 and H_1, L_2 and H_2, and L_3 and H_3, were observed. The intensities at L_2 and H_2 increased with $\boldsymbol{E}\perp\boldsymbol{B}$ and remarkably decreased with $\boldsymbol{E}\|\boldsymbol{B}$ in neat ethanol (Fig. 4). As the laser induces the transition to the $^1\pi\pi^*$ state, $\boldsymbol{E}$ should be located within the xy plane ($\boldsymbol{E}\|x, y$; Fig. 1). From these facts, the L_2 and H_2 fields are assigned to be at $\boldsymbol{B}\|z$, meaning that T_z has the second highest energy and lies at the lowermost ($D > 0$) or uppermost ($D < 0$) position among three sublevels. In acidic ethanol (Fig. 5) although the changes in the spectra were not remarkable, the outermost L_1 and H_1 peaks were assigned to be at $\boldsymbol{B}\|z$ by the same reason, where T_z has the largest absolute energy ($|Z| > |X|,|Y|$). In both cases, the inner-most peaks L_3 and H_3 slightly decreased their intensities with $\boldsymbol{E}\|\boldsymbol{B}$.

In ethanol with ethyl iodide, the similar TREPR spectrum was observed to that in neat ethanol both for polarization and for zfs'.

Table 1. Vibrational Analyses of the Phosphorescence Spectrum of 3,3′-Biisoquinoline in Various Solvents

Ethanol		Acidic ethanol[a]		C_2H_5I added ethanol[b]	
$\tilde{\nu}_{0-0}$ / cm^{-1}	$\Delta\tilde{\nu}$[c]	$\tilde{\nu}_{0-0}$ / cm^{-1}	$\Delta\tilde{\nu}$[c]	$\tilde{\nu}_{0-0}$ / cm^{-1}	$\Delta\tilde{\nu}$[c]
19670	0 (m)	19200	0 (m)	19650	0 (s)
	510 (a′) (m)				510 (a′) (m)
	870 (a″) (s)		880 (s)		870 (a″) (w)
	1450 (a′) (m)		1460 (m)		1440 (a′) (m)
	1600 (a′) (m)				1600 (a′) (m)
					1940 (510+1440) (a′) (w)
	2110 (510+1600) (a′) (m)				2110 (510+1600) (a′) (w)
	2330 (870+1450) (a″) (m)		2330 (880+1460) (m)		

a) Including 2.02 wt% H_2SO_4. b) Including 12.1 wt% ethyl iodide (C_2H_5I). c) a′, a″ band; See Ref. 41.; Intensity; w: weak, m: medium, s: strong.

Table 2. Observed and Calculated EPR Parameters of 3,3′-Biisoquinoline

Solvent			*X*/GHz	*Y*/GHz	*Z*/GHz	$P_x-P_z : P_y-P_z$	*D* /GHz[d]	*E* /GHz[e]
Ethanol	Obsd	(A)	2.070[b]	−0.220[b]	−1.850	0.15 : 0.85	2.775	1.145
		(B)	0.220[b]	−2.070[b]	1.850	0.45 : 0.55[c]	−2.775	1.145
(*trans*)	Calcd		2.238	−0.305	−1.933	— : —	2.900	1.272
Acidic ethanol[a]	Obsd	(A)	0.985[b]	0.785[b]	−1.770	0.45 : 0.55	2.655	0.100
		(B)	−0.785[b]	−0.985[b]	1.770	0.15 : 0.85[c]	−2.655	0.100
(*cis*)	Calcd		1.112	0.854	−1.966	— : —	2.949	0.129

a) Including 2.02 wt% H_2SO_4. b) $X-Y>0$ was assumed. c) $P_y-P_x : P_z-P_x$. d) $D\equiv(-3/2)Z$. e) $E\equiv(X-Y)/2$.

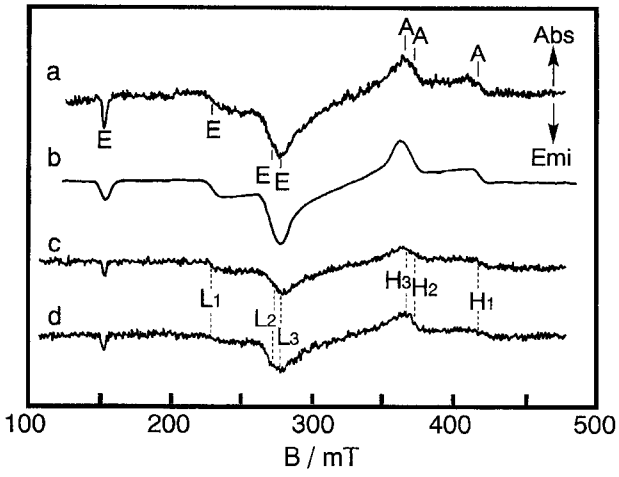

Fig. 5. Time-resolved EPR spectrum (a) of 3,3′-biisoquinoline observed in acidic ethanol with H_2SO_4 (2.02 wt%) at 73 K and 0.8 μs, the simulation spectrum (b) using parameters summarized in Table 2, and magnetophotoselection spectra under excitations with (c) $\boldsymbol{E}\perp\boldsymbol{B}$ and (d) $\boldsymbol{E}\|\boldsymbol{B}$ at 308 nm.

1.3. Theoretical Calculation of zfs. The zfs parameters *D* and *E* were calculated for the *trans* and *cis* conformers of *i*-biq by the method of Higuchi,[27] which was applied to assign the T_1 conformers of 2,2′-(1,2-ethenediyl)bispyridine.[28] The optimized geometry was calculated with the PM3 method in the MOPAC (ver. 3.8)[29] program package and was used for the following MO calculations. The wavefunction of the T_1 state was obtained from the PPP calculation including CI over all one electron excitation configurations. The *D* and *E* values were calculated from Eqs. 1 and 2, respectively:

$$D=-\frac{3}{4}(\mu_0/4\pi)(g\beta)^2\int\phi_{T_1}\cdot\frac{3z^2-R^2}{R^5}\phi_{T_1}\mathrm{d}v_1\mathrm{d}v_2, \quad (1)$$

$$E=-\frac{3}{4}(\mu_0/4\pi)(g\beta)^2\int\phi_{T_1}\cdot\frac{x^2-y^2}{R^5}\phi_{T_1}\mathrm{d}v_1\mathrm{d}v_2. \quad (2)$$

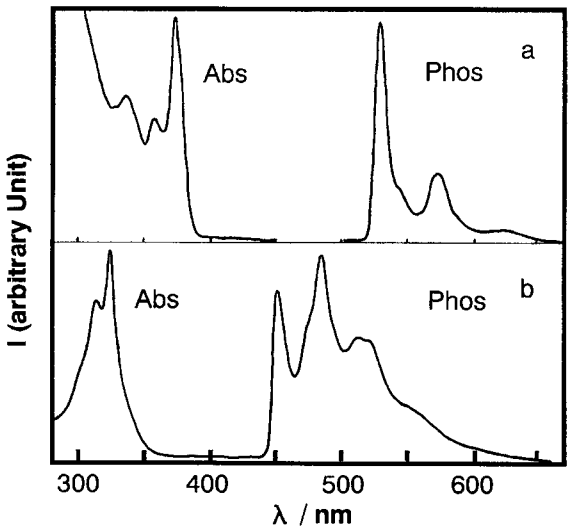

Fig. 6. Absorption (Abs) and Phosphorescence (Phos) spectra observed in dimethylformamide at room temperature and 77 K, respectively for (a) [Pt(CN)$_2$(*i*-biq)] and (b) [Pt(CN)$_2$(bpy)].

Table 3. Energy of the 0–0 Band for S_1 and T_1 and Phosphorescence Lifetime of [Pt(CN)$_2$(*i*-biq)]

Solvent	S_1/cm^{-1}	T_1/cm^{-1}	τ/ms[c]
Dimethylformamide	26300	19000	1.94±0.04
Ethanol/toluene (1 : 1)[a]	26400	19000	2.11±0.02
Acidic ethanol/toluene (1 : 1)[b]	26400	19000	2.31±0.02

a) 1 : 1 by volume. b) Including 10.7 wt% H_2SO_4. c) Obtained at 77 K.

Here ϕ_{T_1} denotes the electronic wavefunction of the T_1 state. The obtained values are measurably different from *trans* to *cis* forms, especially for the *E* value, as summarized in Table 2. The value of θ in Fig. 1 is calculated as 43°.

2. [Pt(CN)$_2$(*i*-biq)]. In the analyses of the T_1 properties of the complex, the locations of the lowest singlet and triplet $d\pi^*$ states are very important. As these states, however, are higher than the lowest $^{1,3}\pi\pi^*$ states and the energies cannot be determined directly from their optical data, the locations of the $^{1,3}d\pi^*$ states in the bpy complex are employed.[16,30,31] The EPR parameters and the isc ratio were obtained from the analyses of the TREPR spectra.

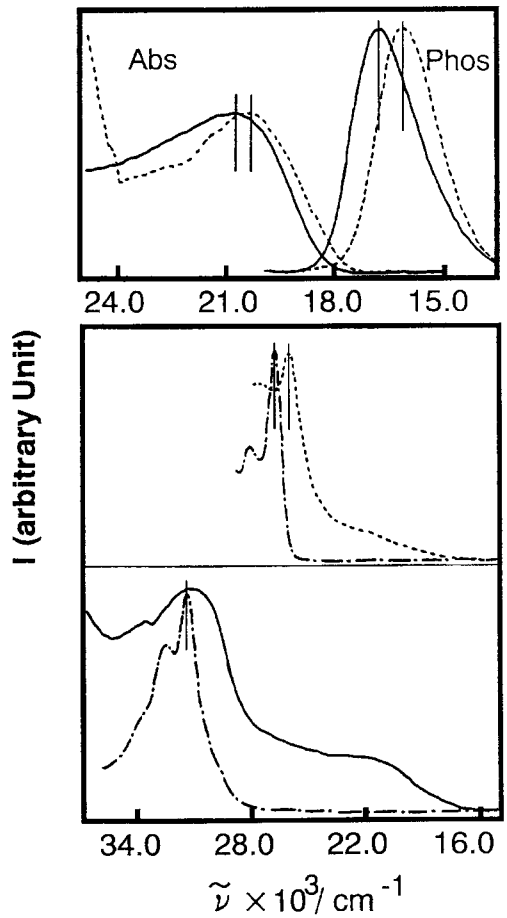

Fig. 7. Absorption (Abs) and Phosphorescence (Phos) spectra of the red form of [Pt(CN)$_2$(*i*-biq)] (- - -) and the red form of [Pt(CN)$_2$(bpy)] (——) observed in the neat crystal and those (– · –) in dimethylformamide at room temperature. The bars indicate peaks of the spectra.

2.1. Optical Properties. Phosphorescence and absorption spectra of the *i*-biq complex were obtained at 77 K and at room temperature, respectively, in DMF, ethanol/toluene (1 : 1 by volume), and acidic ethanol/toluene (1 : 1) including 10.7 wt% H_2SO_4. The typical spectra are shown in Fig. 6(a). The triplet lifetime was determined from the decay of the phosphorescence in these solvents at 77 K, as summarized in Table 3, where the T_1 energy remains nearly the same (ca. 19000 cm^{-1}) and the lifetime (1.9—2.3 ms) is longer in more protic solvent. The absorption spectrum indicates a $\pi\pi^*$ character for S_1 having ε_{max} = 19500 mol^{-1} dm^3 cm^{-1}, which is shifted a little to the blue in more protic solvent. It is found from these data that both the S_1 and T_1 states show dominant $\pi\pi^*$ characters with a little mixed $d\pi^*$ character. In the neat crystal, new broad peaks appeared in the longer wavelength regions both for the absorption and emission (Fig. 7) observed at room temperature. The emission spectra have already been reported in the literature and are assigned to those of the $^{1,3}d_\sigma\pi^*$ (d_σ(Pt) → π^*(*i*-biq)) states.[31] An absorption edge overlaps with the phosphorescence and is assigned as that of the $T_1(d_\sigma\pi^*)$ state.

In order to determine the locations of $^{1,3}d\pi^*$ in the monomeric *i*-biq complex, we made the same experiments for the bpy complex. In DMF, phosphorescence and absorption spectra were obtained as shown in Fig. 6(b). The triplet lifetime was obtained as 65 μs at 77 K. From the structured emission spectrum and the triplet lifetime, the T_1 state is also assigned to be $\pi\pi^*$ in nature. For the absorption spectrum, the peak of ε_{max} = 19000 mol^{-1} dm^3 cm^{-1} at 320 nm is assigned to that of $S_2(\pi\pi^*)$. The longer wavelength part (330—360 nm) having ε = 4500—100 mol^{-1} dm^3 cm^{-1} is assigned to include $S_1(d\pi^*)$ and $T_2(d\pi^*)$ by referring to those of the other Pt complexes.[32–34] The absorption spectrum was simulated by a sum of the single Gaussian curve for the $^1\pi\pi^*$ and the double Gaussian curve for both the $^{1,3}d\pi^*$ states, as shown in Fig. 8. In the neat crystal the absorption

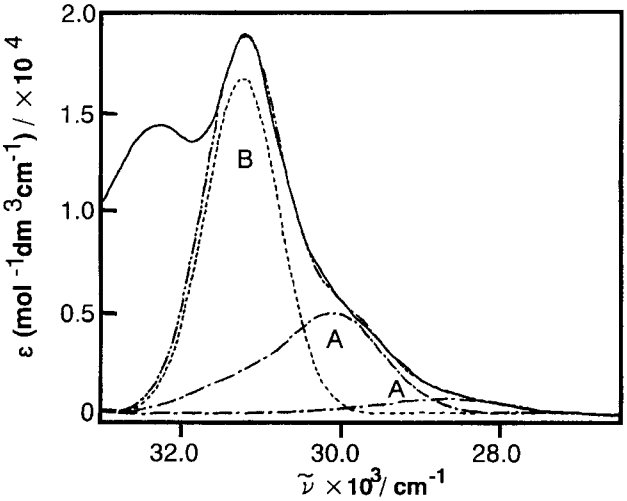

Fig. 8. Absorption spectra (——) of [Pt(CN)$_2$(bpy)] in dimethylformamide at room temperature and fitted curves (– ·· –) with two Gaussian (– · –) lineshapes A and one Gaussian (- - -) B.

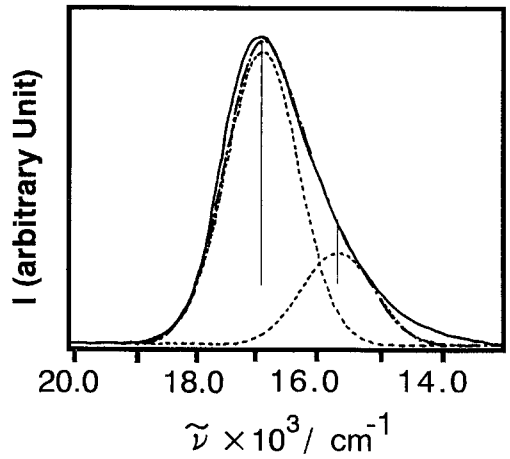

Fig. 9. Observed Phosphorescence spectrum (——) of the red form of $[Pt(CN)_2(bpy)]$ in the neat crystal at room temperature, fitted curves with two Gaussian lineshapes (- - -), and the total curve (– • –).

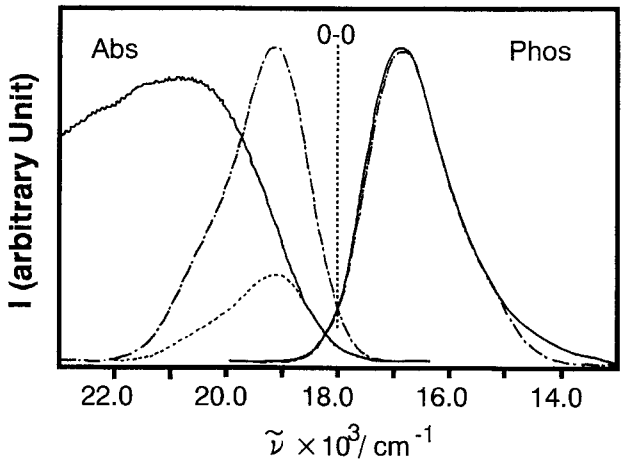

Fig. 10. Location of the 0–0 band determined from the overlap between the fitted curves (– • –) of phosphorescence (Phos) and absorption (Abs) spectra in the neat red crystal of $[Pt(CN)_2(bpy)]$. The curve (– • –) in the absorption spectrum is obtained from the dotted curve (- - -) and normalized with respect to the phosphorescence peak.

and emission spectra (Fig. 7) for the red form of the bpy complex are very similar to those of the red form of the *i*-biq complex at room temperature. These spectra are assigned to be due to the $^{1,3}d_\sigma\pi^*$ ($d_\sigma(Pt) \rightarrow \pi^*(bpy)$) states. The double Gaussian curve is obtained from the analysis of the phosphorescence spectrum of the $^3d_\sigma\pi^*$ in the neat crystal,[35,36] where the spacing (1250 cm^{-1}) of the two Gaussians (Fig. 9) is similar to that (1300 cm^{-1}) of the Pt bpy complexes.[30] The 0–0 energy was evaluated to be lower than that of the Gaussian peak by 1100 cm^{-1}, which was determined from an overlap of the normalized absorption and emission spectra in the neat crystal (Fig. 10).

From these data, it is concluded that $S_1(d\pi^*)$ and $T_2(d\pi^*)$ of the bpy complex locate at 29000 and 27600 cm^{-1}, respectively, in DMF solution. We will discuss the locations of these states for the *i*-biq complex in the following section.

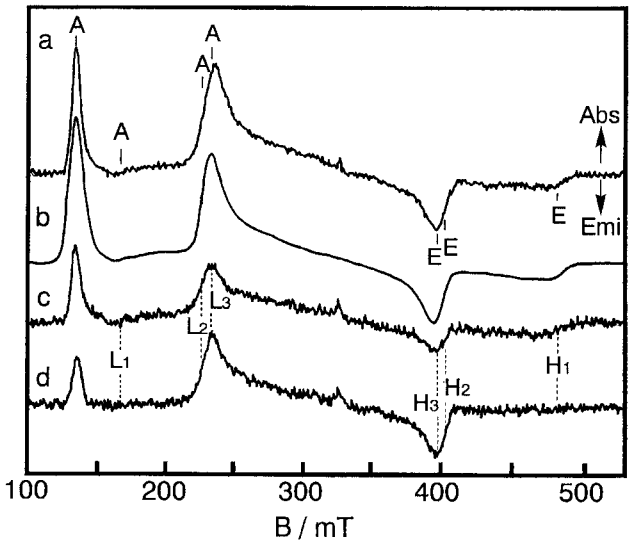

Fig. 11. Time-resolved EPR spectrum (a) of $[Pt(CN)_2(i\text{-biq})]$ observed in ethanol/toluene (1 : 1 by volume) at 110 K and 0.8 μs. The simulation spectrum (b) using parameters summarized in Table 4 and magnetophotoselection spectra under excitations with (c) $\boldsymbol{E} \perp \boldsymbol{B}$ and (d) $\boldsymbol{E} \| \boldsymbol{B}$ at 308 nm.

2.2. EPR Properties. TREPR spectra of the *i*-biq complex were obtained at 20—120 K under various concentrations (5×10^{-6}—5×10^{-4} mol dm^{-3}) in the three solvents; a typical spectrum is shown in Fig. 11. No temperature or concentration dependences were observed in these systems. The polarization pattern shows an A, AAA/EEE type and is quite different from those of the ligand (Fig. 5). A spectral region becomes wider, indicating a larger zfs parameter in the complex. In order to assign triplet sublevels, the MPS experiment was made in the same way as for *i*-biq. The polarized laser pulse of 308 nm excites the complex to the $\pi\pi^*$ state of $\varepsilon = 19000$ mol^{-1} dm^3 cm^{-1}, whose transition moment lies within the *xy* plane ($\boldsymbol{E} \| x, y$). The MPS spectra with $\boldsymbol{E} \| \boldsymbol{B}$ and $\boldsymbol{E} \perp \boldsymbol{B}$ are shown in Fig. 11. From the spectra, it is found that the intensities increase in the inner two sets of the magnetic fields, L_2 and H_2 and L_3 and H_3, and decrease remarkably at the outer most L_1 and H_1 fields with $\boldsymbol{E} \| \boldsymbol{B}$. With $\boldsymbol{E} \perp \boldsymbol{B}$, the L_1 and H_1 peaks increase their intensities. Therefore, the outermost peaks turn out to correspond to the magnetic fields at $\boldsymbol{B} \| z$ and the T_z energy gives the maximum principle value ($|Z| > |X|, |Y|$). Discrimination of the T_x and T_y sublevels was not possible in this experiment.

The spectra were simulated in the three solvents by two parameter sets summarized in Table 4; $D \equiv (-3/2)Z > 0$ and $D < 0$ are again possible. From the solvent dependence of the $|D|$ value, it was found that $|D|$ decreases in more protic solvent, as also summarized in Table 4. The determination of a sign of D is made in the next section.

Discussion

1. Conformation and Sublevel Scheme of *i*-biq. We first discuss the isc rate (k_i) of the triplet sublevel T_i based on the mechanisms of radiationless transitions, determine the dominant path, and assign the triplet sublevel by comparing

Table 4. Obtained EPR Parameters of $[Pt(CN)_2(i\text{-biq})]$

Solvent		X/GHz[c]	Y/GHz[c]	Z/GHz	$P_y-P_x : P_z-P_x$	D/GHz[e]	E/GHz[f]	g_{xx}, g_{yy}	g_{zz}
Dimethylformamide	(A)	1.665	1.445	−3.110	0 : 1.0	4.655	0.110	2.001	2.002
	(B)	−1.445	−1.665	3.110	0.5 : 0.5[d]	−4.655	0.110	2.001	2.002
Ethanol/toluene (1 : 1)[a]	(A)	1.595	1.445	−3.040	0 : 1.0	4.560	0.075	2.001	2.002
	(B)	−1.445	−1.595	3.040	0.5 : 0.5[d]	−4.560	0.075	2.001	2.002
Acidic ethanol/toluene (1 : 1)[b]	(A)	1.540	1.410	−2.950	0 : 1.0	4.425	0.065	2.001	2.002
	(B)	−1.410	−1.540	2.950	0.5 : 0.5[d]	−4.425	0.065	2.001	2.002

a) 1 : 1 by volume. b) Including 10.7 wt% H_2SO_4. c) $X-Y>0$ was assumed. d) $P_x-P_z : P_y-P_z$. e) $D\equiv(-3/2)Z$. f) $E\equiv(X-Y)/2$.

the results with those of zfs' calculated for the *trans* and *cis* isomers.

In the case of nitrogen-heteroaromatics, the $^{1,3}n\pi^*$ states are important as perturbing states in the $S_1(\pi\pi^*) \rightarrow T_1(\pi\pi^*)$ isc process as in the following:

$$k_i = (2\pi/h)| < \psi_{S1}|H_{SO}+H_{TN}|\psi_{T1i} > |^2 \delta(E_v(S_1) - E_{v'}(T_1)) \quad (3)$$

$$\begin{aligned} &< \psi_{S1}|H_{SO}+H_{TN}|\psi_{T1i} > \\ &\quad =< \varphi^0_{S1}(\pi\pi^*)S|H_{SO}|\varphi^0_{T1}(\pi\pi^*)T_i > \\ &+\frac{< \varphi^0_{S1}(\pi\pi^*)|H_{TN}|\varphi^0_{S2}(n\pi^*) >< \varphi^0_{S2}(n\pi^*)S|H_{SO}|\varphi^0_{T1}(\pi\pi^*)T_i >}{E(S_2)-E(S_1)} \\ &+\frac{< \varphi^0_{S1}(\pi\pi^*)S|H_{SO}|\varphi^0_{T2}(n\pi^*)T_i >< \varphi^0_{T2}(n\pi^*)|H_{TN}|\varphi^0_{T1}(\pi\pi^*) >}{E(T_2)-E(S_1)}, \end{aligned} \quad (4)$$

where H_{SO} and H_{TN} are the Hamiltonians for soc and a kinetic energy of nuclei. Total wavefuctions ψ_{S1} and ψ_{T1i} are written as a product form, $\psi_{S1} = \varphi_{S1}S$ and $\psi_{T1i} = \varphi_{T1}T_i$, where S and T_i $(i = x, y, z)$ are spin functions and φ_n $(n = S_1, S_2, T_1, T_2)$ can be expressed as $\varphi_n = \phi_n\chi$, where ϕ_n and χ are electronic and vibrational wavefunctions, respectively. It is well-known that the first term in Eq. 4 is negligibly small because of the three center terms involved.[37,38] In the second and third terms, the selectivity in isc of the triplet sublevel is determined by the matrix elements of soc, Eq. 5.

$$\begin{aligned} &\sum_i < \varphi_{S2}(n\pi^*)S|H_{SO}|\varphi_{T1}(\pi\pi^*)T_i > \\ &= (1/2) < c_x p^N_x + c_y p^N_y|\zeta_1 l_{1x} - \zeta_2 l_{2x}|\sum_n c_n p^n_z >< S|s_{1x} - s_{2x}|T_x > \\ &+(1/2) < c_x p^N_x + c_y p^N_y|\zeta_1 l_{1y} - \zeta_2 l_{2y}|\sum_n c_n p^n_z >< S|s_{1y} - s_{2y}|T_y > . \end{aligned} \quad (5)$$

Here the π and n orbitals are described by

$$\pi = \sum_n c_n p^n_z, \quad (6)$$

$$n = c_x p^N_x + c_y p^N_y, \quad (7)$$

where c_n $(n = 1,2,\cdots)$ denotes the coefficient of the atomic orbitals of C and N. From Eq. 5 it is found that T_z is the least active sublevel $(P_x, P_y > P_z)$ in the $S_1 \rightarrow T_1$ isc process, which is realized in most of the $\pi\pi^*$ triplets in nitrogen-heteroaromatics. Then sublevel scheme A in Table 2 is selected and compared with those of the calculated zfs'. The obtained D values are satisfactorily consistent with the calculated ones including the sign of $D > 0$ (Table 2). We, therefore, conclude that the sublevel ordering is $T_x > T_y > T_z$ in energy for both isomers, where the *trans* form is dominantly observed in neat ethanol and the *cis* in acidic ethanol. The different polarizations observed for the *trans* and *cis* forms are explained in terms of a difference in the sublevel scheme with different populations and splittings.

As for θ in *trans* (Fig. 1), the value is obtained as 37° from the following equation[39] based on Eqs. 3, 4, 5, 6, and 7:

$$P_x/P_y = \sin^2(60^\circ - \theta)/\cos^2(60^\circ - \theta) = 0.15/0.85. \quad (8)$$

This value is reasonably consistent with the calculated value (43°). For the *cis* conformer, the fine structure axes are expected to be parallel to the symmetry axes. The following equation is derived for P_x/P_y:

$$P_x/P_y = \sin^2 60^\circ / \cos^2 60^\circ = 3. \quad (9)$$

As this value is very different from the obtained one (0.8), the $^{1,3}\sigma\pi^*$ states are important instead of $^{1,3}n\pi^*$ states in this case. This might be due to the blue shifts of the $^{1,3}n\pi^*$ states in the acidic solvent. As for the influence of the $^{1,3}n\pi^*$ states on the zfs parameters of T_1, a very weak contribution is expected, because the zfs' are determined by the spin–spin interactions in nitrogen-heteroaromatics.[39] Actually, Yagi et al. have reported negligibly small effects of protonation on the zfs' of T_1 dipyridylethylene.[40]

For the geometry of the *cis*-conformer, the MOPAC calculation for the protonated form, the experimental results of the vibrational structure in the phosphorescence (Table 1) and the relative isc ratio (Table 2), and the coincidence between the calculated and obtained zfs' (Table 2) do all support a nearly planar structure. The conformer in the system of ethyl iodide/ethanol solution is assigned as the trans-form based on the zfs scheme and the triplet energy (Tables 1 and 2). The short lifetime and the enhancements of totally-symmetric vibrations (a′ in Table 1)[41] in the phosphorescence spectrum are interpreted in terms of an external heavy atom effect.[42]

2. Excited States of $[Pt(CN)_2(i\text{-biq})]$. On the basis of the optical and EPR measurements, the following results were obtained for the *i*-biq complex:

1. The zfs $|D|$ value increases with complex formation.

2. The g_{xx} and g_{yy} values are smaller than g_{zz}.

3. The T_z sublevel provides the maximum principal value ($|Z| > |X|, |Y|$).

4. Two kinds of the sublevel schemes are possible: $D \equiv (-3/2)Z > 0$ with $P_z > P_x, P_y$(A) and $D < 0$ with $P_x, P_y > P_z$ (B), as summarized in Table 4.

5. The triplet decay rate and $|D|$ are smaller in the protic solvent. We first discuss the changes in the D and g values and the isc ratio with complex-formation based on an energy level diagram and determine the sublevel scheme. Next we obtain magnitudes of the spin-orbit coupling involved and excitation delocalization over the Pt atom and interpret the effect of solvent.

2.1 Lowest dπ* States and Molecular Orbitals. As Pt(II) has $5d^8$ configuration and is in low spin state, the complex has one vacant 5d orbital, which is considered to be d_{xy} based on electronic interactions with the ligand (Fig. 1). In the extended Hückel MO calculation, the d_{xy} energy is the highest and far from the others, and $d_{x^2-y^2}$ is the most stabilized orbital. Therefore, we consider three kinds of d orbitals (d_{zx}, d_{yz}, d_{z^2}) involved in the lower dπ* states. Due to the symmetry, d_{zx} and d_{yz} orbitals mix with the π and π* orbitals of the ligand, whereas d_{z^2} orbital with the σ character does not mix with those orbitals. Then the π orbital is described by

$$\pi = \sum_n c_n p_z^n + c_{zx} d_{zx} + c_{yz} d_{yz}, \tag{10}$$

where c_n ($n = 1,2,\cdots$) denotes the coefficient of the atomic orbital.

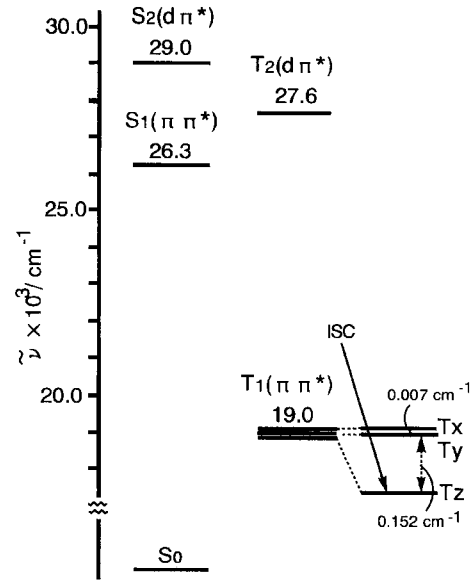

Fig. 12. Energy level diagram of the excited states of [Pt(CN)$_2$(*i*-biq)] including the zero-field splittings of $T_1(\pi\pi^*)$.

2.2. Energy Levels of the dπ* States. Although the energies of the $^{1,3}\pi\pi^*$ states are determined directly from the optical spectra for the *i*-biq complex in solution, those of the $^{1,3}d\pi^*$ states cannot be obtained. In the bpy complex, these dπ* energies were determined from the phosphorescence excitation and absorption spectra, as shown in the previous section. In contrast, the $^{1,3}d_\sigma\pi^*$ states are observed as the lowest excited states in both neat crystals, owing to the strong Pt···Pt interaction. We try to determine the $^{1,3}d\pi^*$ energies of the *i*-biq complex in solution by comparing these data.

In the neat crystal of the *i*-biq complex, the spectral peak of the $^1d_\sigma\pi^*$ locates at ca. 450 cm^{-1} lower in energy than that of the bpy complex (Fig. 7). This differences is interpreted by the shifts of the π* energies in two complexes; the $^1\pi\pi^*$ states are red-shifted from solution to crystal by ca. 800 and 200 cm^{-1} for the *i*-biq and bpy complexes, respectively (Fig. 7). Then the d and $^1d\pi^*$ energy are determined to be nearly the same for the bpy and *i*-biq complexes. This conclusion is supported by the fact that the distance between Pt···Pt is almost the same (3.34 Å)[10,43] at room temperature and a similar energy shift of the d orbital is expected for both complexes with crystal formation.[44] From the phosphorescence peaks in the neat crystals (Fig. 7), we calculate that the $^3d_\sigma\pi^*$ state is lower for the *i*-biq complex by ca. 700 cm^{-1} than that for the bpy complex. Although we do not know the exact amounts of the change in the $^3\pi\pi^*$ energy by crystal formation in the triplet states, 700 cm^{-1} is considered to be comparable to 450 cm^{-1} in the singlet states. Therefore, the $^3d\pi^*$ energy is again estimated to be the same for the both complexes.

On the basis of these discussions, the energies of the $S_2(d\pi^*)$ and $T_2(d\pi^*)$ states in the *i*-biq complex are determined as 29000 and 27600 cm^{-1} in solution, respectively, as summarized in Fig. 12. These states are located a little far from the T_1 state (19000 cm^{-1}).

2.3. Assignment of Triplet Sublevel. Here we determined the sublevel scheme based on the discussion of the isc rate and the change in the D value (Table 4) with complex formation. The ΔD ($\equiv D$(complex)$-D$(*cis*-ligand)) value is considered to come from the contribution of soc as described by Eq. 11.[45,46]

Table 5. Matrix Element of the Spin-Orbit Coupling on the Pt Atom Appeared in Eq. 12[a)]

Intermediate state	First term	Second term	Third term
$d_{zx}\pi^*$ or $d_{yz}\pi^*$	$c_{zx}c_{yz}\zeta <d_{zx}\|l_z\|d_{yz}> ; P_z$	$c_{zx}\zeta <d_{yz}\|l_z\|d_{zx}> ; P_z$ $c_{yz}\zeta <d_{zx}\|l_z\|d_{yz}> ; P_z$	$c_{zx}\zeta <d_{yz}\|l_z\|d_{zx}> ; P_z$ $c_{yz}\zeta <d_{zx}\|l_z\|d_{yz}> ; P_z$
$d_{z^2}\pi^*$	$c_{zx}c_{yz}\zeta <d_{zx}\|l_z\|d_{yz}> ; P_z$	$c_{yz}\zeta <d_{z^2}\|l_x\|d_{yz}> ; P_x$ $c_{zx}\zeta <d_{z^2}\|l_y\|d_{zx}> ; P_y$	$c_{yz}\zeta <d_{z^2}\|l_x\|d_{yz}> ; P_x$ $c_{zx}\zeta <d_{z^2}\|l_y\|d_{zx}> ; P_y$

a) $\zeta = \zeta_{Pt}$; spin-orbit coupling parameter on Pt.

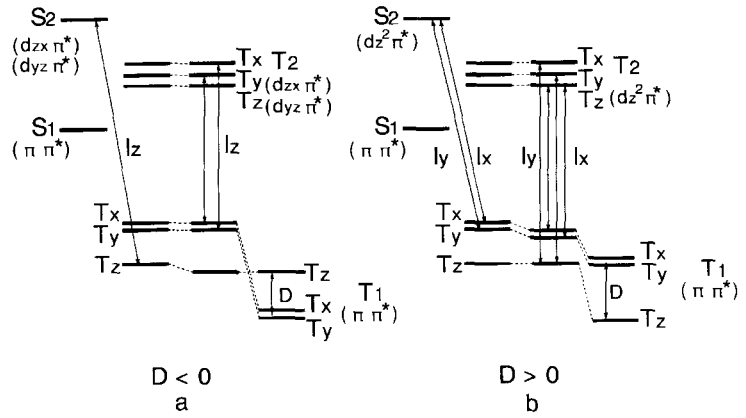

Fig. 13. Two possible interaction schemes of (a) $D < 0$ and (b) $D > 0$ for T_1 [$Pt(CN)_2$(i-biq)].

$$\Delta D = \frac{|<\varphi_{T1}(\pi\pi^*)T_i|H^i_{SO}|\varphi_{S2}(d\pi^*)S>|^2}{E(S_2)-E(T_1)} - \frac{|<\varphi_{T_1}(\pi\pi^*)T_i|H^k_{SO}|\varphi_{T_2}(d\pi^*)T_j>|^2}{E(T2)-E(T_1)}. \quad (11)$$

The change in the spin–spin interaction is negligible, because very small amounts of π and π^* electrons are delocalized over the Pt atom, as obtained in 2.4. The isc rate constant k_i is expressed identically as Eq. 3. Here the matrix element determines sublevel selectivity as described by

$$\begin{aligned}&<\psi_{S1}|H_{SO}+H_{TN}|\psi_{T1i}>\\ &=<\varphi^0_{S1}(\pi\pi^*)S|H_{SO}|\varphi^0_{T1}(\pi\pi^*)T_i>\\ &+\frac{<\varphi^0_{S1}(\pi\pi^*)|H_{TN}|\varphi^0_{S2}(d\pi^*)><\varphi^0_{S2}(d\pi^*)S|H_{SO}|\varphi^0_{T1}(\pi\pi^*)T_i>}{E(S_2)-E(S_1)}\\ &+\frac{<\varphi^0_{S1}(\pi\pi^*)S|H_{SO}|\varphi^0_{T2}(d\pi^*)T_i><\varphi^0_{T2}(d\pi^*)|H_{TN}|\varphi^0_{T1}(\pi\pi^*)>}{E(T_2)-E(S_1)}.\end{aligned} \quad (12)$$

In this case, as the first term includes the one center term on Pt because of contamination of the d character in the π orbital (Eq. 10), all three terms in Eq. 12 should be considered for three kinds of d orbitals: d_{zx}, d_{yz}, and d_{z^2}. The matrix elements of soc which appear in these equations are summarized in Table 5.

We discuss the two possible sets of P_i and D (Table 4) for two cases, **a**; d = d_{zx} and/or d_{yz} and **b**; d = d_{z^2}. In case **a**, $P_z > P_x$, P_y is expected for all three terms in Eq. 12. The obtained P_i is the relative value of k_i. For the sublevel energy, T_z is stabilized by the interaction with $S_2(d\pi^*)$ and T_x and T_y are stabilized with $T_2(d\pi^*)$, as illustrated in Fig. 13(a). When the energy denominator is considered for these two states, the latter contribution prevails over the former, making T_x and T_y lower in energy and giving $D < 0$ ($D \equiv (-3/2)Z$). This is not consistent with either of the two possible schemes and case **a** does not explain the experimental results.

In case **b**, the first term in Eq. 12 gives rise to $P_z > P_x$, P_y and the second and third terms give P_x, $P_y > P_z$. For the D value, T_x and T_y are stabilized by the interaction with $S_2(d\pi^*)$ and T_z is more stabilized with $T_2(d\pi^*)$ (Fig. 13(b)). Due to the smaller energy denominator again for the latter, T_z is stabilized more, giving $D > 0$. This expectation together with the one ($P_z > P_x$, P_y) from the first term of Eq. 12 is consistent with the experimental results of scheme A in Table 4 and scheme b in Fig. 13. This fact indicates that the direct soc term is more important in this complex. Now the sublevel scheme and the dominant isc route are determined as shown in Fig. 12 and the $^{1,3}d_{z^2}\pi^*$ states are found to be most important perturbing states for the T_1 properties of the complex.

2.4. Spin Density on Pt and g Value. From the above discussion, the values of ΔD (= −0.0667 cm^{-1}), $E(S_2)-E(T_1)$ (= 10000 cm^{-1}), and $E(T_2)-E(T_1)$ (= 8600 cm^{-1}) are obtained. These values give rise to the magnitude of the soc matrix element $|<{}^3\pi\pi^*|H^i_{SO}|^{1,3}d\pi^*>|$ ($i = x, y$) as 65 cm^{-1} from Eq. 11 and the assumption that the values are same for the $^{1,3}d\pi^*$ states. Using Eq. 13 and $\zeta_{Pt} = 4000$ cm^{-1}, the delocalization coefficients c_{yz} and c_{zx} of the π^* electrons over the d_{zx} and d_{yz} orbitals on Pt (Eq. 10) are obtained as 0.02.

$$\begin{aligned}&<\varphi_{S2}(d^2_z\pi^*)S|H^i_{SO}|\varphi_{T1}(\pi\pi^*)T_i>\\ &=(1/2)<d_{z^2}\pi^*|\zeta_{Pt}(l_{1i}-l_{2i})|\pi\pi^*><S|s_{1i}-s_{2i}|T_i>\\ &=(c_{zx})\zeta_{Pt}<d_{z^2}|l_y|d_{zx}>/2=c_{zx}\zeta_{Pt}\sqrt{3/2} \qquad (i=y)\\ &=-c_{yz}\zeta_{Pt}\sqrt{3/2}. \qquad (i=x)\end{aligned} \quad (13)$$

The g_{ii} ($i = x,y,z$) value is changed by soc with the $T_2(d_{z^2}\pi^*)$ state as described by[45,46]

$$\Delta g_{ii} = g_{ii} - g_e = \frac{-2\sum_i <\varphi_{T1}(\pi\pi^*)|l_i|\varphi_{T2}(d_{z^2}\pi^*)><\varphi_{T2}(d_{z^2}\pi^*)T_j|H^i_{SO}|\varphi_{T1}(\pi\pi^*)T_k>}{E(T_2)-E(T_1)}. \quad (14)$$

When g_e (= 2.0023), $E(T_2)-E(T_1)$, and the soc matrix element of 65 cm^{-1} are used, Δg_{xx} and Δg_{yy} are obtained as −0.0005 and $\Delta g_{zz} = 0$. The experimentally obtained values (Table 4) nicely coincide with these estimated ones, which again supports the importance of the $^3d_{z^2}\pi^*$ state for the $T_1(\pi\pi^*)$ property.

2.5. Solvent Effect. The correlation between the triplet decay rate and the D value was found from the results in three solvents (Tables 3 and 4). These results are interpreted by the blue shifts of the $^{1,3}d\pi^*$ states in protic solvent. As the $^{1,3}\pi\pi^*$ states shift little (< 100 cm^{-1}) in these solvents,

the magnitudes of the change in the ΔD value from that in DMF, 3.2×10^{-3} cm^{-1} (ethanol/toluene) and 7.7×10^{-3} cm^{-1} (acidic ethanol/toluene), provide the energy shifts of 230 and 600 cm^{-1}, respectively for the $^{1,3}d\pi^*$ states. These values are consistent with those for [Pt(CN)$_2$(bpy)] in ethanol (520 cm^{-1}) and acidic ethanol (850 cm^{-1}), which are obtained from the UV-vis absorption spectra.

Conclusion

1. The *trans* and *cis* forms of the ligand *i*-biq were assigned in the T_1 state in ethanol and acidic ethanol solution, respectively, on the basis of the obtained and calculated zero-field splitting parameters.

2. For the complex of [Pt(CN)$_2$(*i*-biq)], the energy levels of the $^{1,3}\pi\pi^*$ states were assigned spectroscopically and those of $^{1,3}d\pi^*$ were estimated by comparing the optical spectra with those of [Pt(CN)$_2$(bpy)].

3. The triplet sublevels of the *i*-biq complex were assigned from the analyses of the spin-orbit coupling between $T_1(\pi\pi^*)$ and the $^{1,3}d\pi^*$ states and the $S_1 \rightarrow T_1$ intersystem crossing ratio.

4. The magnitudes of the matrix element of spin-orbit coupling involved and the electron delocalization over the Pt atom were obtained as 65 cm^{-1} and as 0.02, respectively, in the $T_1(\pi\pi^*)$ state of [Pt(CN)$_2$(*i*-biq)].

5. Solvent dependences of the zero-field splitting and the triplet lifetime were analyzed by the blue shifts of the $^{1,3}d\pi^*$ states.

References

1 A. Juris, V. Balzani, F. Barigelletti, S. Campagna, P. Belser, and A. V. Zelewsky, *Coord. Chem. Rev.*, **84**, 85 (1988).

2 V. Balzani, A. Juris, M. Venturi, S. Campagna, and S. Serroni, *Chem. Rev.*, **96**, 759 (1996).

3 Y. Komada, S. Yamauchi, and N. Hirota, *J. Phys. Chem.*, **90**, 6425 (1986).

4 A. P. Suisalu, A. L. Kamyshnyi, V. N. Zakharov, L. A. Aslanov, and R. A. Avarmaa, *Chem. Phys. Lett.*, **134**, 617 (1987).

5 H. Miki, M. Shimada, T. Azumi, J. A. Brozik, and G. A. Crosby, *J. Phys. Chem.*, **97**, 11175 (1993).

6 H. Miki, S. Kimachi, R. Satomi, T. Azumi, and M. Onishi, *Chem. Phys. Lett.*, **218**, 563 (1994).

7 M. Yagi, A. Saitoh, K. Takano, K. Suzuki, and J. Higuchi, *Chem. Phys. Lett.*, **118**, 275 (1985).

8 M. Yagi, B. D. Schlyer, and A. H. Maki, *Chem. Phys.*, **157**, 209 (1991).

9 M. Yagi, T. Kaneshima, T. Wada, K. Takemura, and Y. Yokoyama, *J. Photochem. Photobiol. A: Chem.*, **84**, 27 (1994).

10 M. Kato, K. Sasano, C. Kosuge, M. Yamazaki, S. Yano, and M. Kimura, *Inorg. Chem.*, **35**, 116 (1996).

11 R. D. Haworth and S. Robinson, *J. Chem. Soc.*, **1948**, 777.

12 B. R. Harriman, R. S. Shelton, M. G. V. Campen, and M. R. Warren, *J. Am. Chem. Soc.*, **67**, 1481 (1945).

13 A. R. Osborn and K. Schofield, *J. Chem. Soc.*, **1956**, 4191.

14 M. Tiecco, M. Tingoli, L. Testaferri, D. Chianelli, and E. Wenkert, *Tetrahedron*, **42**, 1475 (1986).

15 W. T. Brady, *Synthesis*, **1971**, 415.

16 C. -M. Che, L. -Y. He, C. -K. Poon, and T. C. W. Mak, *Inorg. Chem.*, **28**, 3081 (1989).

17 K. Nakamoto, *J. Phys. Chem.*, **64**, 1420 (1960).

18 R. H. Linnell and A. Kaczmarczyk, *J. Phys. Chem.*, **65**, 1196 (1961).

19 M. Yagi, Y. Deguchi, Y. Shioya, and J. Higuchi, *Chem. Phys. Lett.*, **144**, 412 (1988).

20 J. Higuchi, M. Yagi, T. Iwaki, M. Bunden, K. Tanigaki, and T. Ito, *Bull. Chem. Soc. Jpn.*, **53**, 890 (1980).

21 M. Yagi, K. Makiguchi, A. Ohnuki, K. Suzuki, J. Higuchi, and S. Nagase, *Bull. Chem. Soc. Jpn.*, **58**, 252 (1985).

22 L. L. Merritt, Jr., and E. D. Schroeder, *Acta Crystallogr.*, **9**, 801 (1956).

23 R. H. Clarke, P. Mitra, and K. Vinodgopal, *J. Chem. Phys.*, **77**, 5288 (1982).

24 L. A. Summer, "Advances in Heterocyclic Chemistry," ed by A. R. Katritzky Frs, Academic Press, New York (1984), Vol. 35, pp. 281—374.

25 S. T. Howard, *J. Am. Chem. Soc.*, **118**, 10269 (1996).

26 P. Belser, A. V. Zelewsky, A. Juris, F. Barigelletti, A. Tucci, and V. Balzani, *Chem. Phys. Lett.*, **89**, 101 (1982).

27 J. Higuchi, *Bull. Chem. Soc. Jpn.*, **54**, 2864 (1981).

28 Y. Shioya, K. Mikuni, J. Higuchi, and M. Yagi, *J. Phys. Chem.*, **98**, 12521 (1994).

29 J. J. P. Stewart, *J. Comput. Chem.*, **10**, 209 (1989).

30 V. M. Miskowski and V. H. Houlding, *Inorg. Chem.*, **30**, 4446 (1991).

31 M. Kato, C. Kosuge, K. Morii, J. S. Ahn, H. Kitagawa, T. Mitani, M. Matsushita, T. Kato, S. Yano, and M. Kimura, *Inorg. Chem.*, **38**, 1638 (1999).

32 P. M. Gidney, R. D. Gillard, and B. T. Heaton, *J. Chem. Soc., Dalton Trans.*, **1973**, 132.

33 V. M. Miskowski and V. H. Houlding, *Inorg. Chem.*, **28**, 1529 (1989).

34 V. M. Miskowski, V. H. Houlding, C. -M. Che, and Y. Wang, *Inorg. Chem.*, **32**, 2518 (1993).

35 The reason why the solid and solution $^3d\pi^*$ spectra are assumed to be same is based on a previous result that the phosphorescence spectra are nearly the same for [Ru(*i*-biq)$_3$](PF$_6$)$_2$ in DMF and in the neat crystal. See Ref. 36.

36 M. Kato, K. Sasano, M. Kimura, and S. Yamauchi, *Chem. Lett.*, **1992**, 1887.

37 M. A. El-Sayed, *Acc. Chem. Res.*, **4**, 23 (1971).

38 M. A. El-Sayed, *Ann. Rev. Phys. Chem.*, **26**, 235 (1975).

39 J. Schmidt, W. S. Veeman, and J. H. van der Waals, *Chem. Phys. Lett.*, **4**, 341 (1969).

40 M. Noda, K. Matsushima, K. Seki, and M. Yagi, *Chem. Phys. Lett.*, **296**, 599 (1998).

41 S. C. Wait, Jr., and J. C. Mcnernet, *J. Mol. Spectrosc.*, **34**, 56 (1970).

42 Y. Komada, S. Yamauchi, and N. Hirota, *J. Chem. Phys.*, **82**, 1651 (1985).

43 W. B. Connick, L. M. Henling, and R. E. Marsh, *Acta Crystallogr., Sect. B*, **B52**, 817 (1996).

44 G. Gliemann and H. Yersin, *Struct. Bond.*, **62**, 87 (1985).

45 M. Batley and R. Bramley, *Chem. Phys. Lett.*, **15**, 337 (1972).

46 N. M. Atherton, "Principles of Electron Spin Resonance," Ellis Horwood and Prentice Hall Press, New York (1993).